Kang et al. *Zool. Res. Divers. Conserv.* 2025, 2(3): 175−181
https://doi.org/10.24272/j.issn.2097-3772.2025.020
https://cstr.cn/32249.14.zrdc.2025.020

ZRDC Zoological Research: Diversity and Conservation

Article Open Access

Climatic and genetic factors shape geographic color variation in the Guinan toad-headed lizard (*Phrynocephalus guinanensis*)

Da Kang[1,2,3], Xia Qiu[4], Zhong-Yi Yao[1,2], Ying Chen[1,2,3], Yin Qi[1,2], Song Tan[1,2], Wei-Zhao Yang[1,2,*]

[1] *Mountain Ecological Restoration and Biodiversity Conservation Key Laboratory of Sichuan Province*, *Chengdu Institute of Biology*, *Chinese Academy of Sciences*, *Chengdu*, *Sichuan* 610213, *China*

[2] *China-Croatia Belt and Road Joint Laboratory on Biodiversity and Ecosystem Services*, *Chengdu Institute of Biology*, *Chinese Academy of Sciences*, *Chengdu*, *Sichuan* 610213, *China*

[3] *University of Chinese Academy of Sciences*, *Beijing* 100049, *China*

[4] *College of Life Sciences*, *China Jiliang University*, *Hangzhou*, *Zhejiang* 310018, *China*

ABSTRACT

Coloration constitutes one of the most striking features of phenotypic diversity in animals, yet the evolutionary mechanisms underlying its diversification remain incompletely resolved, particularly in species expressing multiple distinct color traits. The Guinan toad-headed lizard (*Phrynocephalus guinanensis*), endemic to the Mugetan Desert region, exhibits pronounced ventral color polymorphism, including black, red (restricted to males), and green (restricted to females), offering a robust system to investigate the ecological and genetic drivers of coloration divergence. To identify the ecological and genetic factors governing this variation, ventral coloration was quantified in 137 individuals across 15 populations using standardized spectrophotometry and calibrated digital imaging. Generalized linear models incorporating bioclimatic data and population genetic structure showed that black pigmentation was strongly associated with mean annual temperature, consistent with a role in thermoregulation. In contrast, red and green coloration varied with population genetic structure in both sexes, suggesting divergence shaped by sexual selection. These results indicate that both climatic and genetic factors have together shaped the geographic color variation in this species, providing deeper insight into the evolutionary dynamics and diversity of animal coloration.

Keywords: Animal coloration; *Phrynocephalus guinanensis*; Climatic factors; Genetic structure; Evolutionary drivers

INTRODUCTION

The striking diversity of coloration observed across animal taxa has long captivated biologists (Caro et al., 2017; Caro & Mallarino, 2020; Cuthill et al., 2017), yet the mechanisms driving its evolution remain incompletely understood. Coloration fulfills a range of adaptive functions, including camouflage, intra- and interspecific communication, aposematism, and regulation of body temperature, and thus plays a central role in mediating organismal interactions with both biotic and abiotic environments (Dunn et al., 2015; Mackintosh, 2001; McLean et al., 2014; Refsnider et al., 2018). As one of the most visually prominent traits shaping human perception of biological biodiversity, color variation provides a valuable framework for investigating the evolutionary mechanisms that drive its diversification and contribute to the emergence of broader phenotypic diversity (Delhey et al., 2023).

Animal coloration frequently varies across climatic and environmental gradients (Gomez & Théry, 2004; Marchetti, 1993; Zeuss et al., 2014), reflecting spatial shifts in its functional roles (Cooney et al., 2022; Gomez & Théry, 2004). For instance, lighter pigmentation is typically favored in warmer environments, where reduced solar absorption confers thermal advantage, while darker forms dominate in cooler regions due to more efficient heat retention (Zeuss et al., 2014). Beyond climatic influences, genetic relatedness can constrain color evolution by limiting developmental trajectories and promoting conservation of ancestral patterns

Received: 03 August 2025; Accepted: 16 October 2025; Online: 11 November 2025

Foundation items: This study was supported by the National Natural Science Foundation (32370459 and 32400381), TianFu Emei Plan Youth Talent Project in Science and Technology (2023-7), Sichuan Provincial International Science and Technology Cooperation Initiative (2024YFHZ0247), and Second Round Central Forestry Reform and Development Fund (QHPG-2023-036).

*Corresponding author, E-mail: yangwz@cib.ac.cn

(Arbore et al., 2024; Kaelin et al., 2025; Toh et al., 2025). In Papilionidae, for instance, aposematic coloration remains phylogenetically conserved, reflecting strong genetic retention of ancestral traits (Condamine et al., 2015; Jiggins et al., 2001; Zhang et al., 2017). However, most empirical work has focused on single color traits in isolation (Endler, 2012; Guan et al., 2024), leaving unresolved how multiple, co-occurring color traits are simultaneously shaped by environmental and genetic factors. This gap limits understanding of the mechanisms governing the origin and diversification of complex color phenotypes.

The Guinan toad-headed lizard (*Phrynocephalus guinanensis*) provides an excellent model for investigating how evolutionary processes have shaped complex coloration traits (Figure 1A, B). This species occupies a narrow range within the Mugetan Desert and adjacent regions along the northeastern margin of the Qinghai-Xizang Plateau (Ji et al., 2009). Its ventral surface features three distinct coloration elements, including a black belly patch and sexually dichromatic ventrolateral color expressed as red in males and green in females (Chen et al., 2025; Condamine et al., 2015; Xiao et al., 2024). More importantly, these traits vary markedly across their distribution range. Individuals inhabiting the central desert consistently express the characteristic black, red, and green pigmentation, whereas populations on the northern gravel substrate habitat outside the desert exhibit a gradual shift toward white ventral coloration (Xiao et al., 2024). Substantial heterogeneity also occurs near the desert boundary, where individuals frequently express only a single color trait, such as isolated black or isolated red ventral patches. Functional studies indicate that these color components contribute to multiple ecological roles. For instance, the ventral black region accelerates heat gain under solar radiation, consistent with a thermoregulatory function (Jin et al., 2016), while the red ventrolateral coloration in males predicts outcomes of male-male competitive interactions (Xiao et al., 2024). Despite these advances, the factors underlying the emergence and maintenance of this geographically structured color variation remain elusive.

This study quantified geographic variation in all three ventral pigmentation traits in *P. guinanensis* by integrating color measurements, climatic variables, and genetic data for 137 individuals sampled across 15 sites. Generalized linear models (GLMs) and hierarchical partitioning were applied to determine how the three color traits are distributed across the study area, and the extent to which climatic gradients and population genetic structure account for this geographic variation and their relative contributions.

MATERIALS AND METHODS

Animal ethics

All animal collection protocols complied with national regulations in China and adhered to institutional guidelines for animal care and use. Field sampling was approved by the Forestry and Grassland Bureau of Qinghai Province, China, and the Ethical Committee for Animal Experiments at Chengdu Institute of Biology, Chinese Academy of Sciences (Approval No. CIBDWLL2022025).

Sampling

Fieldwork was carried out from May to August during the years 2022–2024 in Mugetan Desert and adjacent northern

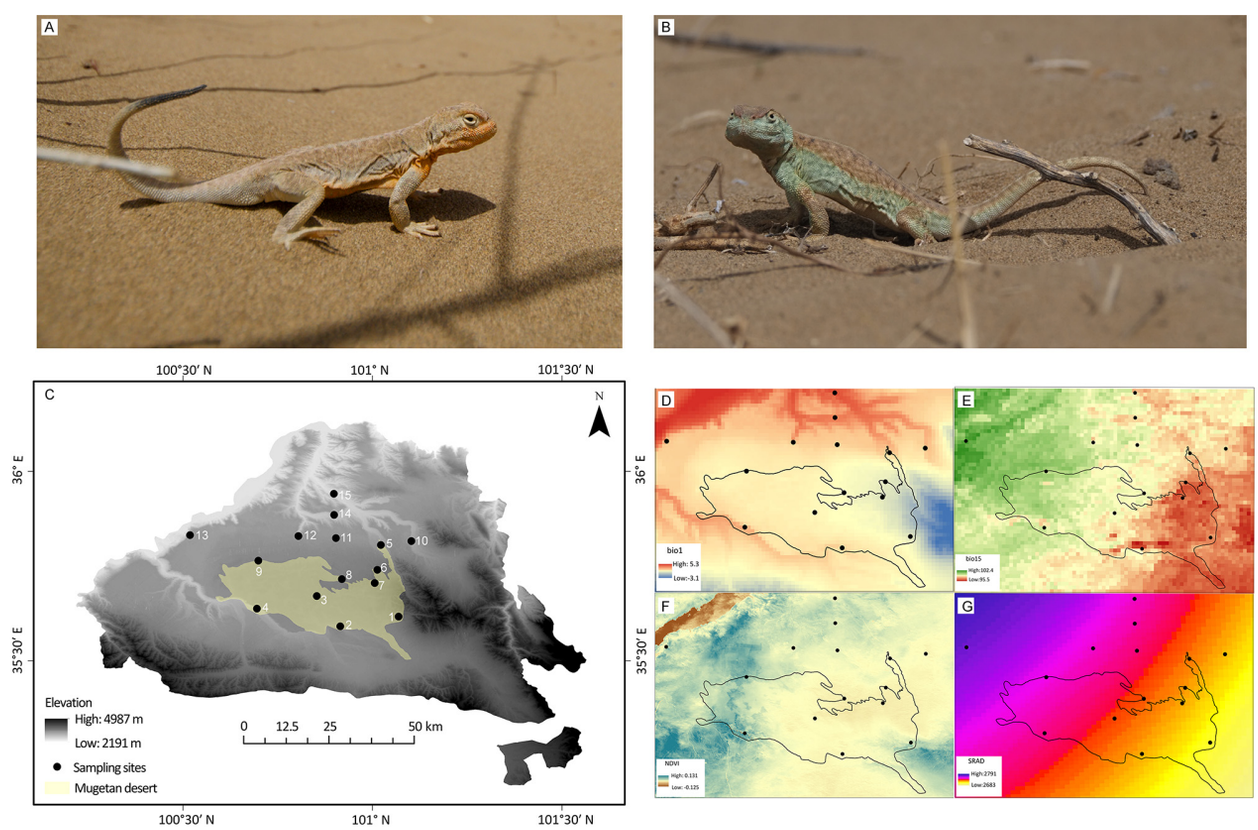

Figure 1 Photographs of male and female *Phrynocephalus guinanensis* individuals and the study site

A: Photograph of a representative male. B: Photograph of a representative female. C: Mugetan Desert range. Black dots represent study sampling sites. D–G: Distribution patterns of four climatic factors (bio1, bio15, NDVI, and SRAD) at study sites.

regions (N35.55°–N35.95°, E100.50°–E101.12°). A total of 137 adult *P. guinanensis* individuals, including 72 males and 65 females, were collected from 15 sites (Figure 1C; Supplementary Table S1). Based on habitat features, sites were categorized into three types: sand dune habitat within the desert (IN; sites 1–4), northern gravel substrate habitat outside the desert (OUT; sites 10–15), and transitional ecotone region in the middle (MID; sites 5–9). Sampling was conducted on consecutive sunny days between 9:00 and 15:00, coinciding with peak activity periods for *Phrynocephalus* lizards (Kang et al., 2024). Individuals were captured using a lasso, followed by measurement of morphological and coloration traits. All lizards were released to their original capture sites after data collection.

Color quantification

Coloration was quantified using trait-specific methods tailored to the distinct characteristics of each pigmentation element. As the black and red traits are expressed as discrete patches, area-based quantification was applied, while the green trait —manifesting as a more continuous hue —was better captured through spectral analysis For black and red coloration, standardized digital photographs of the abdominal surface were taken for each individual using a fixed-angle setup with a Sony α6400 camera (Kanagawa, Japan) and a ColorChecker passport (Calibrite LLC; Wilmington, DE, USA) for color calibration. Image processing was performed using ImageJ v.1.54 (Schindelin et al., 2012) to calculate the total abdominal area (AA), black area (AB) for all individuals, and red region (AR) for males only. The black score was defined as AB/AA×100%, while the red score for males was calculated as AR/(AA−AB)×100%. Green coloration in females was quantified using a Jaz optic spectrophotometer with a PX2 light source (Ocean Optics Inc., Dunedin, FL, USA). Reflectance spectra were collected from six sites on the ventrolateral region (three per side) (Xiao et al., 2024). Measurements were normalized using a 99% white standard (WS-1) and a black reference (Labsphere; North Sutton, NH, USA). Spectral data were analyzed using the R package "*pavo*" (Maia et al., 2013, 2019), and the Hue value (H1) was extracted as the green score. All processed color data are provided in Supplementary Table S2.

Climatic data collection

Geographic coordinates (latitude and longitude) were recorded at each sampling site and used to extract 19 bioclimate variables at 30 arc-second resolution from the WorldClim 2.0 database (Fick & Hijmans, 2017). To reduce multicollinearity impacts on downstream analysis, pairwise Pearson correlation tests were conducted to identify significantly correlated variables (P<0.05; Supplementary Figure S1; Wang et al., 2022). Based on ecological relevance for reptiles (Ruiz Miñano et al., 2021; Sreelatha et al., 2025), two climatic variables were retained, including mean annual temperature (bio1, Figure 1D) and precipitation seasonality (bio15, Figure 1E). Additional environmental predictors included the Normalized Difference Vegetation Index (NDVI), representing ground net primary productivity obtained at a spatial resolution of approximately 1 km from the Environment Science and Data Center (http://www.resdc.cn/) (Figure 1F), and annual direct normal solar radiation (SRAD) extracted from CHELSA v1.2 (Karger et al., 2017) (Figure 1G).

In addition, estimates of food resource availability (FR) were collected at each sampling site. Using the collection point of each individual as the center of a 5 m radius circular plot, all visible potential prey (including Coleoptera and Lepidoptera insects) were counted during a standardized 1 min observation period. Details for all explanatory variables are provided in Supplementary Table S3.

Genetic structure inference

Genetic data were downloaded from the National Genomics Data Center (NGDC) under accession number PRJCA027608. All populations, except sites 3 and 7, which were excluded due to the absence of usable genetic information, were included in the final dataset. Single nucleotide polymorphism (SNP) data were generated following the pipeline described in Chen et al. (2025). Pairwise F_{ST} values were estimated between all population pairs using the R packages "*hierfstat*" (Goudet, 2005) and "*genepop*" (Rousset, 2008) to construct the genetic distance matrix. To assess spatial genetic structure, the correlation between genetic differentiation and geographic distance was evaluated using the R package "*vegan*" (Oksanen et al., 2025). Principal component analysis (PCA) was performed using the "*prcomp*" function in R v4.2.0 (R Core Team, 2022) based on the F_{ST} matrix. The first principal component (PC1) was used to indicate the level of genetic differentiation among populations (Supplementary Table S4).

Statistical analysis

Normality of each color trait was assessed using the Shapiro-Wilk test (Shapiro & Wilk, 1965), and homogeneity of variance was verified using the Bartlett test (P>0.05), satisfying the assumptions of one-way analysis of variance (ANOVA). ANOVA was then used to compare differences in black, red, and green coloration across sampling locations. For traits with significant ANOVA results (P<0.05), *post hoc* comparisons were conducted using the Tukey HSD test to identify pairwise differences while controlling for Type I error inflation from multiple testing (Tukey, 1949).

Although the three color traits differ in biological function and sex-specific expression, a consistent modeling framework was used to assess the effects of identical climatic and genetic predictors. This approach enabled direct comparison across traits by accounting for their distinct statistical properties through the use of appropriate distribution families (see below). Generalized linear models (GLMs) were used to assess the effects of six explanatory variables —bio1 (mean annual temperature), bio15 (precipitation seasonality), NDVI, SRAD, FR, and PC1 of genetic structure—on variation in each color trait of *P. guinanensis*. Each color trait was modeled independently as a response variable. To ensure valid model specification, appropriate probability distributions and link functions were selected based on data normality tests and model fit criteria (AIC/BIC). Black coloration was modeled using a Gaussian distribution with an identity link, while red and green coloration were modeled using Gamma distributions with inverse and log link functions, respectively. Prior to modeling, multicollinearity among predictors was assessed by calculating variance inflation factors (VIFs) using the "*check_collinearity*" function in the R package "*performance*" (Lüdecke et al., 2021). Predictors with VIF>5 were excluded from the full models (Supplementary Table S5). Given the small sample size and the total of 64 possible combinations of six predictors (2^6), model selection was performed using corrected Akaike Information Criterion (AICc) values (Symonds & Moussalli, 2011). All candidate models

were generated using the "*dredge*" function in "*MuMIn*" (Bartoń, 2025), and the best-fitting model was identified by averaging all models with ΔAICc<2 using the "*model.avg*" function in "*MuMIn*" (Bartoń, 2025; Si et al., 2014; Symonds & Moussalli, 2011). Finally, to further quantify the independent contributions of climatic and genetic variables, hierarchical partitioning was conducted using the R package "*glmm.hp*" (Lai et al., 2022, 2023). All statistical analyses were carried out in R v4.2.0 (R Core Team, 2022).

RESULTS

Color traits and genetic structure

Black scores were recorded from 137 individuals, with a mean score of 46.29%±1.28% (SE). Similarly, red scores, obtained from 72 males, averaged 56.12%±3.61% (SE). For green coloration, 65 females were measured, yielding a mean hue score of 599.72±4.29 nm (SE). Overall, all three color traits differed significantly among the IN, OUT, and MID groups (ANOVA, P<0.001, Figure 2). Black scores showed significant differences between all group pairs ($P_{IN\text{-}OUT}$<0.001; $P_{IN\text{-}MID}$=0.006; $P_{MID\text{-}OUT}$<0.001). Red scores differed significantly between OUT and the other two groups ($P_{IN\text{-}OUT}$<0.001; $P_{IN\text{-}MID}$=0.056; $P_{MID\text{-}OUT}$<0.001). Green hue values also differed significantly between OUT and the other two regions ($P_{IN\text{-}OUT}$<0.001; $P_{IN\text{-}MID}$=0.710; $P_{MID\text{-}OUT}$<0.001).

Genetic distance was significantly correlated with geographic distance across all populations (R=0.576; P<0.001). PCA of the pairwise FST matrix showed that PC1 explained 50.76% of the total variance and was used as an indicator of population genetic structure in subsequent modeling.

Evolutionary drivers of color variation

Collinearity analysis indicated that only the red coloration model exceeded the VIF threshold, with elevated values for bio15 (VIF=5.43) and SRAD (VIF=7.70). These two variables were therefore excluded from subsequent red color modeling (Supplementary Table S5). Model selection and averaging yielded two candidate models for black coloration, three for red, and three for green (Table 1). For black coloration, the best-fitting model included bio1 and bio15; black scores showed a significant negative correlation with bio1 (P=0.001) and a marginal positive correlation with bio15 (P=0.051, Table 2). For red coloration, the best-fitting model included bio1 and PC1; red scores increased significantly with bio1 (P=0.034) and showed a positive but non-significant correlation with PC1 (P=0.092, Table 2). For green coloration, the best-fitting model included bio1, bio15, NDVI, and PC1; green scores increased significantly with bio1 (P=0.014) and PC1 (P=0.014) and showed a negative but non-significant correlation with bio15 (P=0.078) and NDVI (P=0.179) (Table 2).

Hierarchical partitioning analysis revealed that the three color traits were shaped by distinct combinations of climatic factors and genetic structure (Figure 3). Black coloration was influenced most strongly by bio1 (45.93%), followed by bio15 (23.92%), SRAD (9.09%), NDVI (9.09%), FR (6.70%), and PC1 (5.26%). Red coloration was driven primarily by PC1 (38.39%) and bio1 (33.93%), with smaller contributions from FR (14.29%) and NDVI (13.39%). Green coloration showed a similar pattern, with PC1 (33.86%) and bio1 (32.67%) accounting for the largest fractions of explained variation, followed by bio15 (15.14%), NDVI (6.77%), FR (5.98%), and SRAD (5.58%).

DISCUSSION

This study investigated the spatial variation of three ventral color traits in *P. guinanensis* and evaluated the extent to which climatic gradients and population genetic structure account for their geographic distributions. Distinct patterns emerged

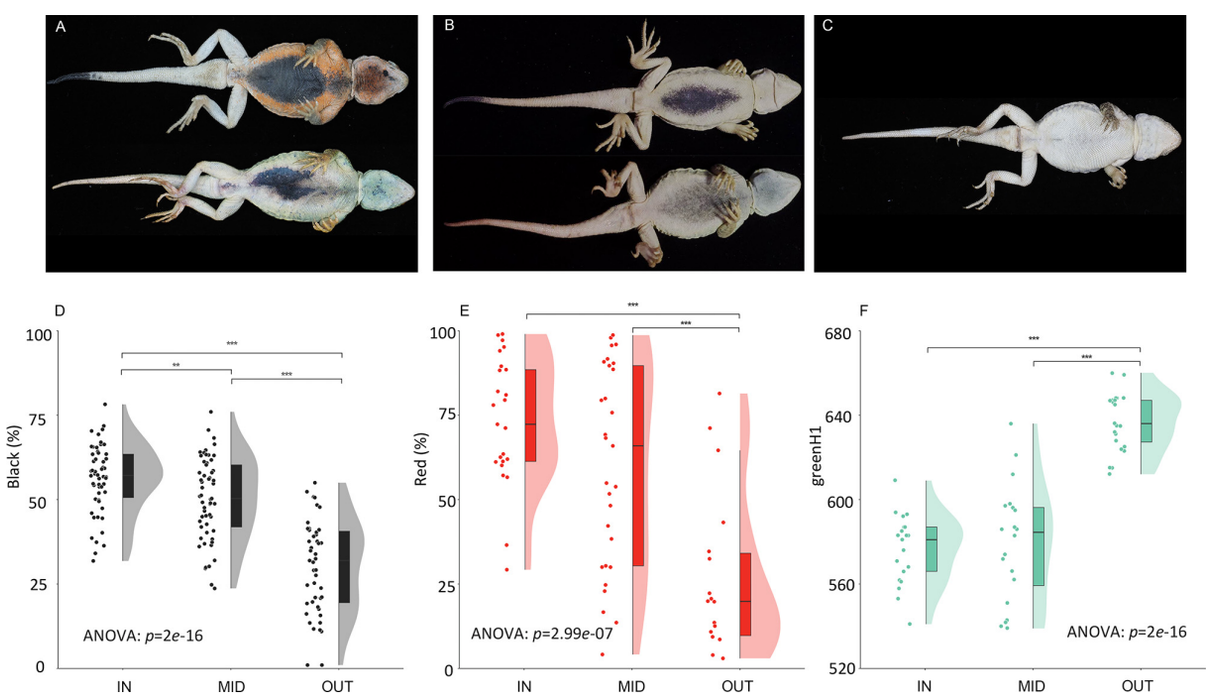

Figure 2 Geographic variation in coloration of *Phrynocephalus guinanensis*

A: Ventral coloration of individuals sampled from desert interior. B: Gradual fading of the three color traits along desert border. C: Uniform white ventral coloration in individuals from non-desert habitats. D–F: Color scores for black, red, and green pigmentation in the IN, MID, and OUT groups, respectively. Asterisks indicate significance levels from ANOVA (*P<0.05; **P<0.01; ***P<0.001).

Table 1 Candidate models with ΔAICc<2 included in model averaging

	Model in confidence set	df	logLik	AICc	ΔAICc	Weight
Black	bio1+bio15	4	−53.453	118.9	0.00	0.347
	bio1	3	−55.940	120.1	1.16	0.195
Red	PC1	3	−68.954	146.1	0.00	0.279
	bio1	3	−69.133	146.4	0.36	0.233
	NULL	2	−71.123	147.2	1.16	0.156
Green	bio1+PC1	4	−62.015	136.0	0.00	0.423
	bio1+bio15+PC1	5	−59.717	136.1	0.07	0.408
	bio1+NDVI+PC1	5	−60.604	137.9	1.84	0.168

Table 2 Averaged top models derived from GLMs evaluating associations between climatic variables, genetic structure, and the three color traits

Model	Operational variable	N. models	Estimate	SE	*Z*-value	*P*-value
Black	Intercept		42.723	2.589	14.900	2e-16*
	bio1	2	−11.469	3.087	3.402	0.001*
	bio15	1	6.094	2.806	1.954	0.051
Red	Intercept		0.022 617	0.003 851	5.405	6e-08*
	bio1	1	0.007 063	0.003 017	2.124	0.033 7*
	PC1	1	0.004 200	0.002 260	1.686	0.091 8
Green	Intercept		6.401 851	0.006 991	819.314	2e-16*
	bio1	3	0.025 658	0.009 379	2.459	0.013 9*
	PC1	3	0.010 231	0.003 743	2.454	0.014 1*
	bio15	1	−0.015 123	0.007 635	1.764	0.077 7
	NDVI	1	−0.012 716	0.008 434	1.343	0.179 4

Note: For each model, the number of models including each explanatory variable (N. models), estimated coefficient (Estimate), standard error (SE), *Z*-value, and *P*-value are reported. Asterisks denote statistical significance. Models with ΔAICc<2 were retained as the most plausible.

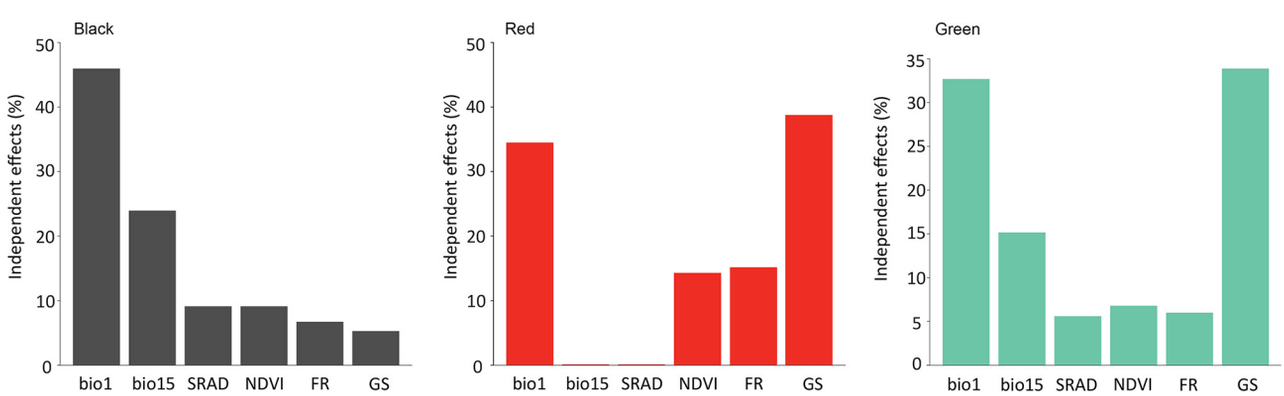

Figure 3 Independent contributions (%) of climatic factors and genetic structure to three color traits, as determined by hierarchical partitioning analysis.

among populations inhabiting desert interiors, peripheral ecotones, and external gravel regions, with all three pigmentation traits differing significantly across these habitat types. Furthermore, climatic variables —particularly mean annual temperature (bio1)—were significantly associated with variation in all color traits, while genetic structure (PC1) also contributed to spatial differentiation of the sexually dichromatic red and green pigmentation. These findings suggest that both environmental selection and genomic divergence have jointly driven the diversification of color traits in *P. guinanensis*, offering broader insights into the mechanisms by which complex coloration systems evolve and are maintained in natural populations.

Climatic factors exerted strong and consistent effects on the spatial distribution of all three color traits in *P. guinanensis*. Mean annual temperature (bio1) emerged as a key predictor in the best-fitting models for each trait, contributing over 30% to explained variance in the hierarchical partitioning analysis and reaching 45.93% for black pigmentation. In fact, it was no surprise that the melanin-based black coloration was substantially correlated with temperature (e.g. Clusella Trullas et al., 2007). In *Adalia bipunctata*, for example, melanic morphs display elevated heating rates compared to non-melanic morphs, as revealed by infrared thermography (Brakefield & Willmer, 1985). Similarly, melanic phenotypes in Eurasian vipers have been linked to colder habitats, where darker individuals gain thermal advantages through more rapid warming (Martínez-Freiría et al., 2020). In *P. guinanensis*, individuals from the desert interior—where mean annual temperatures are lower —exhibited markedly darker ventral pigmentation than those from peripheral or external regions. This pattern likely reflects a thermoregulatory adaptation, supported by physiological evidence showing that the black abdominal region heats more rapidly than adjacent

non-pigmented areas under solar exposure (Jin et al., 2016). Comparable adaptations have been reported in other *Phrynocephalus* species, such as *P. theobaldi*, where black ventral pigmentation is consistently expressed at elevations above 4 200 m, enhancing solar heat absorption in cold alpine environments (Jin & Liao, 2015).

In addition to temperature, precipitation seasonality (bio15) showed a marginally significant association with black coloration (P=0.051), contributing 23.92% in the partitioning analysis. This relationship may reflect an indirect interaction, whereby precipitation-driven humidity fluctuations influence the thermal properties or ecological utility of melanic pigmentation. A similar climate-coloration linkage has been observed in other biological groups, such as Australian birds, where darker plumage correlates with both colder and more humid environments (Delhey, 2018). Collectively, these findings provide robust evidence that climatic variables—especially thermal regimes—play a crucial role in shaping the geographic distribution of color traits in *P. guinanensis*.

Beyond climatic factors, spatial variation in the sexually dichromatic coloration of *P. guinanensis* was closely linked to underlying genetic structure. Green coloration exhibited a significant association with genetic structure in the best-fitting model (P=0.014), accounting for 33.86% of explained variance in hierarchical partitioning. Although the red trait did not reach statistical significance (P=0.092), it remained a prominent contributor in the optimal model, explaining 38.39% of total variance. These findings align with the long-recognized role of genetic relatedness in driving convergent or divergent coloration patterns among populations and closely related species, often shaped by shared ancestry and constrained evolutionary pathways (Condamine et al., 2015; Jiggins et al., 2001). For instance, psittacofulvin-based coloration underlies extensive chromatic diversity among parrots (Arbore et al., 2024), while abdominal setal shifts between orange and black among South Asian *Bombus* species support Müllerian mimicry within regional faunal assemblages (Yang et al., 2023). In *P. guinanensis*, red and green ventral colors are likely under sexual selection during the breeding season (Lu et al., 2024; Xiao et al., 2024), potentially contributing to population-level divergence in mate preference and subsequent genetic differentiation. However, environmental covariation may also influence these traits. Both red and green coloration were associated with mean annual temperature (bio1), while green was also weakly correlated with precipitation seasonality (bio15) and vegetation cover (NDVI). This interplay between sexual selection and environmental filtering has been documented in other ectothermic taxa. For example, in *Podarcis muralis*, male ornamental traits are enhanced in arid, high-temperature environments, consistent with dual pressures of thermoregulation and mate attraction (Ruiz Miñano et al., 2021). Thus, these results suggest that sexually selected coloration in *P. guinanensis* reflects a complex balance between genetic background, climatic factors, and potential ecological trade-offs, warranting further investigation into the mechanistic and evolutionary underpinnings of color divergence across its range.

Pronounced geographic heterogeneity in coloration is often indicative of strong spatially variable selection acting across environmental or social gradients (Cooney et al., 2022; Gomez & Théry, 2004). In *P. guinanensis*, distinct evolutionary pathways appear to govern different color traits. Black coloration showed a robust association with climatic conditions, particularly mean annual temperature, consistent with a thermoregulatory role of melanin under thermal constraint (Goldenberg et al., 2024; Sreelatha et al., 2025). In contrast, the red and green sexually dichromatic traits exhibited significant associations with both climate and genetic structure, suggesting a tradeoff between sexual selection and natural selection (Cooney et al., 2019; Ruiz Miñano et al., 2021). The presence of multiple color traits shaped by distinct combinations of climatic gradients and genetic structure within a geographically restricted range provides novel insights into how animal coloration evolves and diversifies. Nevertheless, the mechanistic links between these coloration traits and external ecological or social factors remain unresolved, underscoring the need for targeted behavioral and physiological investigations to address this gap.

COMPETING INTERESTS

The authors declare that they have no competing interests.

AUTHOR CONTRIBUTIONS

D.K.: Data curation (lead); formal analysis (lead); investigation (equal); writing-original draft (lead). X.Q.: Data curation (equal); investigation (equal); validation (equal). Z.Y.Y.: Validation (equal); data curation (equal). Y.C.: Formal analysis (equal); validation (equal). Y.Q.: Resources (equal); validation (equal). S.T.: Investigation (equal); validation (equal). W.Z.Y.: Funding acquisition (lead); methodology (lead); writing - review and editing (lead); supervision (lead); visualization (lead); investigation (equal). All authors read and approved the final version of the manuscript.

ACKNOWLEDGMENTS

We would like to thank Lin Cui and Qiwei Xu from the Chengdu Institute of Biology, Chinese Academy of Sciences (China), for assistance in field work and photographic sampling. We are grateful to Xiaoyi Wang from the Chengdu Institute of Biology, Chinese Academy of Sciences (China), and Mengchun Jiang from the Sichuan Jintang High School (China) for advice on climate data analysis.

REFERENCES

Arbore R, Barbosa S, Brejcha J, et al. 2024. A molecular mechanism for bright color variation in parrots. *Science*, **386**(6721): eadp7710.

Bartoń K. 2025[2025-04-05]. MuMIn: multi-model inference. https://CRAN.R-project.org/package=MuMIn.

Brakefield PM, Willmer PG. 1985. The basis of thermal melanism in the ladybird *Adalia bipunctata*: differences in reflectance and thermal properties between the morphs. *Heredity*, **54**(1): 9–14.

Caro T, Mallarino R. 2020. Coloration in mammals. *Trends in Ecology & Evolution*, **35**(4): 357–366.

Caro T, Stoddard MC, Stuart-Fox D. 2017. Animal coloration research: why it matters. *Philosophical Transactions of the Royal Society B: Biological Sciences*, **372**(1724): 20160333.

Chen Y, Tan S, Xu QW, et al. 2025. Genomic architecture underlying the striking colour variation in the presence of gene flow for the guinan toad‐headed lizard. *Molecular Ecology*, **34**(1): e17594.

Clusella Trullas S, van Wyk JH, Spotila JR. 2007. Thermal melanism in ectotherms. *Journal of Thermal Biology*, **32**(5): 235–245.

Condamine FL, Toussaint EFA, Clamens AL, et al. 2015. Deciphering the evolution of birdwing butterflies 150 years after Alfred Russel Wallace. *Scientific Reports*, **5**: 11860.

Cooney CR, He YC, Varley ZK, et al. 2022. Latitudinal gradients in avian colourfulness. *Nature Ecology & Evolution*, **6**(5): 622–629.

Cooney CR, Varley ZK, Nouri LO, et al. 2019. Sexual selection predicts the rate and direction of colour divergence in a large avian radiation. *Nature*

Communications, **10**(1): 1773.
Cuthill IC, Allen WL, Arbuckle K, et al. 2017. The biology of color. *Science*, **357**(6350): eaan0221.
Delhey K. 2018. Darker where cold and wet: Australian birds follow their own version of Gloger's rule. *Ecography*, **41**(4): 673–683.
Delhey K, Valcu M, Muck C, et al. 2023. Evolutionary predictors of the specific colors of birds. *Proceedings of the National Academy of Sciences of the United States of America*, **120**(34): e2217692120.
Dunn PO, Armenta JK, Whittingham LA. 2015. Natural and sexual selection act on different axes of variation in avian plumage color. *Science Advances*, **1**(2): e1400155.
Endler JA. 2012. A framework for analysing colour pattern geometry: adjacent colours. *Biological Journal of the Linnean Society*, **107**(2): 233–253.
Fick SE, Hijmans RJ. 2017. WorldClim 2: new 1-km spatial resolution climate surfaces for global land areas. *International Journal of Climatology*, **37**(12): 4302–4315.
Goldenberg J, Bisschop K, Bruni G, et al. 2024. Melanin-based color variation in response to changing climates in snakes. *Ecology and Evolution*, **14**(7): e11627.
Gomez D, Théry M. 2004. Influence of ambient light on the evolution of colour signals: comparative analysis of a neotropical rainforest bird community. *Ecology Letters*, **7**(4): 279–284.
Goudet J. 2005. HIERFSTAT, a package for R to compute and test hierarchical *F*-statistics. *Molecular Ecology Notes*, **5**(1): 184–186.
Guan DF, Sun SY, Song LY, et al. 2024. Taking a color photo: a homozygous 25-bp deletion in *Bace2* may cause brown-and-white coat color in giant pandas. *Proceedings of the National Academy of Sciences of the United States of America*, **121**(11): e2317430121.
Ji X, Wang YZ, Wang Z. 2009. New species of *Phrynocephalus* (Squamata, Agamidae) from Qinghai, Northwest China. *Zootaxa*, **1988**(1): 61–68.
Jiggins CD, Naisbit RE, Coe RL, et al. 2001. Reproductive isolation caused by colour pattern mimicry. *Nature*, **411**(6835): 302–305.
Jin YT, Liao PH. 2015. An elevational trend of body size variation in a cold-climate agamid lizard. *Phrynocephalus theobaldi. Current Zoology*, **61**(3): 444–453.
Jin YT, Tong HJ, Zhang KL. 2016. The impact of phenotypic characteristics on thermoregulation in a cold-climate agamid lizard. *Phrynocephalus guinanensis. Asian Herpetological Research*, **7**(3): 210–219.
Kaelin CB, McGowan KA, Trotman JC, et al. 2025. Molecular and genetic characterization of sex-linked orange coat color in the domestic cat. *Current Biology*, **35**(12): 2826–2836. e5.
Kang D, Zhao CL, Sun ZJ, et al. 2024. Effects of microhabitat features on the intraspecific variability of the distribution and functional traits in a highest elevational distributed lizard. *Ecology and Evolution*, **14**(2): e10902.
Karger DN, Conrad O, Böhner J, et al. 2017. Climatologies at high resolution for the earth's land surface areas. *Scientific Data*, **4**: 170122.
Lai JS, Zhu WJ, Cui DF, et al. 2023. Extension of the *glmm. hp* package to Zero-Inflated Generalized Linear Mixed Models and multiple regression. *Journal of Plant Ecology*, **16**(6): rtad038.
Lai JS, Zou Y, Zhang S, et al. 2022. glmm. hp: an R package for computing individual effect of predictors in generalized linear mixed models. *Journal of Plant Ecology*, **15**(6): 1302–1307.
Lu B, Qiu X, Yang WZ, et al. 2024. Genetic basis and evolutionary forces of sexually dimorphic color variation in a toad-headed agamid lizard. *Molecular Biology and Evolution*, **41**(3): msae054.
Lüdecke D, Ben-Shachar MS, Patil I, et al. 2021. performance: an R package for assessment, comparison and testing of statistical models. *Journal of Open Source Software*, **6**(60): 3139.
Mackintosh JA. 2001. The antimicrobial properties of melanocytes, melanosomes and melanin and the evolution of black skin. *Journal of Theoretical Biology*, **211**(2): 101–113.
Maia R, Eliason CM, Bitton PP, et al. 2013. pavo: an R Package for the analysis, visualization and organization of spectral data. *Methods in Ecology and Evolution*, **4**(10): 906–913.
Maia R, Gruson H, Endler JA, et al. 2019. PAVO 2: new tools for the spectral and spatial analysis of colour in R. *Methods in Ecology and Evolution*, **10**(7): 1097–1107.
Marchetti K. 1993. Dark habitats and bright birds illustrate the role of the environment in species divergence. *Nature*, **362**(6416): 149–152.
Martínez-Freiría F, Toyama KS, Freitas I, et al. 2020. Thermal melanism explains macroevolutionary variation of dorsal pigmentation in Eurasian vipers. *Scientific Reports*, **10**(1): 16122.
McLean CA, Moussalli A, Stuart-Fox D. 2014. Local adaptation and divergence in colour signal conspicuousness between monomorphic and polymorphic lineages in a lizard. *Journal of Evolutionary Biology*, **27**(12): 2654–2664.
Oksanen J, Simpson GL, Blanchet FG, et al. 2025[2025-09-18]. Vegan: community ecology package. http://CRAN.R-project.org/web/packages/vegan/index.html.
R Core Team. 2022. R: a language and environment for statistical computing. R Foundation for Statistical Computing. http://www.R-project.org/.
Refsnider JM, Qian SS, Streby HM, et al. 2018. Reciprocally transplanted lizards along an elevational gradient match light environment use of local lizards via phenotypic plasticity. *Functional Ecology*, **32**(5): 1227–1236.
Rousset F. 2008. GENEPOP' 007: a complete re-implementation of the GENEPOP software for Windows and Linux. *Molecular Ecology Resources*, **8**(1): 103–106.
Ruiz Miñano M, While GM, Yang WZ, et al. 2021. Climate shapes the geographic distribution and introgressive spread of color ornamentation in common wall lizards. *The American Naturalist*, **198**(3): 379–393.
Schindelin J, Arganda-Carreras I, Frise E, et al. 2012. Fiji: an open-source platform for biological-image analysis. *Nature Methods*, **9**(7): 676–682.
Shapiro SS, Wilk MB. 1965. An analysis of variance test for normality (Complete Samples). *Biometrika*, **52**(3-4): 591–611.
Si XF, Pimm SL, Russell GJ, et al. 2014. Turnover of breeding bird communities on islands in an inundated lake. *Journal of Biogeography*, **41**(12): 2283–2292.
Sreelatha LB, Tarroso P, Nokelainen O, et al. 2025. Environmental gradients in lizard colouration. *Ecology and Evolution*, **15**(3): e71012.
Symonds MRE, Moussalli A. 2011. A brief guide to model selection, multimodel inference and model averaging in behavioural ecology using Akaike's information criterion. *Behavioral Ecology and Sociobiology*, **65**(1): 13–21.
Toh H, Au Yeung WK, Unoki M, et al. 2025. A deletion at the X-linked *ARHGAP36* gene locus is associated with the orange coloration of tortoiseshell and calico cats. *Current Biology*, **35**(12): 2816–2825. e3.
Tukey JW. 1949. Comparing individual means in the analysis of variance. *Biometrics*, **5**(2): 99–114.
Wang XY, Zhong MJ, Yang SN, et al. 2022. Multiple β-diversity patterns and the underlying mechanisms across amphibian communities along a subtropical elevational gradient. *Diversity and Distributions*, **28**(12): 2489–2502.
Xiao X, Tan S, He KH, et al. 2024. Pterin-based red coloration predicts the outcome of male–male competition in guinan toad-headed lizard. *Animals*, **14**(20): 2923.
Yang WH, Cui JX, Chen YX, et al. 2023. Genetic modification of a *Hox* locus drives mimetic color pattern variation in a highly polymorphic bumble bee. *Molecular Biology and Evolution*, **40**(12): msad261.
Zeuss D, Brandl R, Brändle M, et al. 2014. Global warming favours light-coloured insects in Europe. *Nature Communications*, **5**: 3874.
Zhang W, Westerman E, Nitzany E, et al. 2017. Tracing the origin and evolution of supergene mimicry in butterflies. *Nature Communications*, **8**(1): 1269.